Lattice Boltzmann algorithm to simulate isotropic-nematic emulsions

N. Sulaiman,[1] D. Marenduzzo,[2] and J. M. Yeomans[1]
[1]*Rudolf Peierls Centre for Theoretical Physics, 1 Keble Road, Oxford, OX1 3NP, United Kingdom*
[2]*SUPA, School of Physics, University of Edinburgh, Mayfield Road, Edinburgh EH9 3JZ, United Kingdom*
(Received 1 March 2006; revised manuscript received 26 July 2006; published 27 October 2006)

We present lattice Boltzmann simulations of the dynamical equations of motion of a drop of isotropic fluid in a nematic liquid crystal solvent, both in the absence and in the presence of an electric field. The coupled equations we solve are the Beris-Edward equations for the dynamics of the tensor order parameter describing the nematic solvent, the Cahn-Hilliard equation for the concentration evolution, and the Navier-Stokes equations for the determination of the instantaneous velocity field. We implement the lattice Boltzmann algorithm to ensure that spurious velocities are close to zero in equilibrium. We first study the effects of the liquid crystal elastic constant, K, anchoring strength, W, and surface tension, σ, on the shape of the droplet and on the director field texture in equilibrium. We then consider how the drop behaves as the director field is switched by an applied electric field. We also show that the algorithm allows us to follow the motion of a drop of isotropic fluid placed in a liquid crystal cell with a tilted director field at the boundaries.

DOI: 10.1103/PhysRevE.74.041708 PACS number(s): 77.84.Nh, 61.30.Jf, 61.30.−v

I. INTRODUCTION

Our aim in this paper is to describe a lattice Boltzmann algorithm which solves the equations of motion of a liquid crystalline phase coexisting with an isotropic liquid. This is a first step towards investigating problems such as the hydrodynamics of nematic emulsions, phase ordering in nematic-isotropic mixtures and the switching behavior of coexisting nematic and isotropic fluids in liquid crystal devices. Here we use the algorithm to follow the hydrodynamics of a drop of isotropic fluid within a nematic as the alignment of the director is rotated by an external electric field and to show how the drop can be moved across a nematic cell by a patterned surface.

Emulsions are dispersions of liquid droplets in a continuous liquid solvent. A type of emulsion, which has particularly interesting properties, is made up of isotropic droplets dispersed into uniformly aligned nematic liquid crystals. The introduction of the drops leads to the formation of topological defects in the liquid crystal close to the droplet surface. These defects mediate anisotropic droplet-droplet interactions that typically lead to ordered droplet structures, such as chains and hexagonal lattices [1–6] (see however Ref. [7] for the case of nanodroplet emulsions). Recent work has also shown interesting behavior as the drops approach a free nematic surface: director deformations caused by the droplets lead to distortions of the interface and thus to capillary attraction [8]. Moreover, there have been suggestions that nematic emulsions could prove useful in liquid crystal devices, for example, as electrically switchable light modulators [9].

Due to a considerable body of experimental and theoretical research the static properties of liquid crystal emulsions are now rather well understood. Isotropic droplets, with normal anchoring of the director field at their surface, are normally accompanied by a hyperbolic hedgehog defect of dipolar symmetry to satisfy the far field alignment [1,2]. Weaker surface anchoring, a smaller drop, or the application of an electric field tends to stabilize a Saturn ring defect of quadrupolar symmetry [10–12]. In two dimensions the stable configuration is a defect pair of topological charge $-1/2$ located symmetrically around the particle [13].

Nematic-isotropic mixtures also show unexpected effects when subject to a temperature quench. Loudet *et al.* [3] reported experiments on a system quenched from a single-phase nematic to a two-phase region where an isotropic and a nematic phase coexisted. Isotropic drops grew to a certain size, but then growth was arrested and the drops formed chains. Numerical simulations of a quench in a symmetric liquid-crystal–isotropic mixture led to an asymmetric pattern of disconnected nematic domains as a result of the coupling between the director field and the flow field [14].

Park *et al.* [15] have investigated drops of isotropic fluid suspended in nematic phase under an applied field. Drops of isotropic fluid are deformed into an elliptical shape perpendicular to the field. The deformations were larger than that found in nonliquid crystal systems due to small surface tension.

Most numerical work so far has focused on elucidating the director field in the vicinity of the isotropic droplet. Molecular dynamic simulations have been used to examine the disclination structure for very small droplets [16–18]. Other authors have addressed larger length scales by minimizing a Landau-de Gennes free energy functional, with either the director field or Q tensor as order parameter. Defect structures have been mapped out for a disc [13] or sphere [19,20], for a confined particle [21], for a disc near a free nematic surface [22] and for a pair of spherical particles [23]. Monte Carlo simulations have led to similar results [24,25].

Although the equilibrium properties of isotropic-nematic mixtures are well studied there has been very little work on the hydrodynamic and phase ordering behavior of these systems. Molecular dynamics is able to explore the dynamical behavior but is restricted to very small length and short time scales [18]. Fukuda *et al.* [26] have investigated the effect of hydrodynamic flow on the orientational order of the nematic liquid crystal around a fixed particle with a hyperbolic hedgehog defect. It would be interesting to have a tool to explore further the rheology of nematic emulsions which is

expected to be strongly viscoelastic. Therefore here we describe a lattice Boltzmann algorithm which solves the hydrodynamic equations of motion of a nematic coexisting with an isotropic phase. These are demanding simulations and therefore we restrict ourselves to two dimensions. Similar equations are considered in Ref. [14] and solved using an explicit Euler scheme. The interface between isotropic and nematic fluids has been investigated using the lattice Boltzmann scheme that recovers the Qian-Sheng equations by Care *et al.* [27] who investigated the shape of a droplet of an isotropic fluid immersed in a nematic liquid crystal in the presence of a surfactant [28].

In Sec. II we describe the free energy functional that we shall use to describe the equilibrium properties of the two-component nematic-isotropic system. We also summarize the equations of motion for the mixtures. Section III describes the lattice Boltzmann method and how it can be extended to nematic-isotropic mixtures. Sections IV–VI present results of the simulations. First we investigate how the interplay between elastic energy, surface coupling, and surface tension affects the shape of the drop. We then investigate the coupling between the movement of the director field and the drop as the director is rotated by an external electric field. We also consider how a drop of isotropic fluid moves to the walls of a cell if there is a suitably patterned director field at the surface. Section VII summarizes the results and concludes the paper.

II. THE MODEL

In this section we summarize a model which describes the equilibrium phase behavior and hydrodynamics of a binary mixture of an isotropic liquid and a lyotropic liquid crystal. We first write down the Landau-de Gennes free energy that corresponds to the system under investigation. The hydrodynamics is described by the Beris-Edwards equations of motion for nematic liquid crystals [29] coupled to Cahn-Hilliard dynamics for the diffusion of the two species. In Sec. III we introduce a lattice Boltzmann algorithm which solves these equations.

A. Free energy and thermodynamic quantities

The system we consider is a mixture of an isotropic liquid and a liquid crystal. Its free energy depends on two order parameters, ϕ, the liquid crystal concentration, and $\mathbf{Q}$, a tensor describing the liquid crystalline order. We write the total free energy $\mathcal{F}(\phi,Q)$ as

$$\mathcal{F} = \int_V dV\{f_{\text{bulk}} + f_{\text{el}} + f_E + f_{\kappa_\phi} + f_W\} + \int_S dS f_a. \tag{1}$$

The bulk free energy f_{bulk} is

$$f_{\text{bulk}}(\phi,Q) = f_{\text{mix}}(\phi) + f_{\text{ani}}(\phi,Q), \tag{2}$$

where f_{mix} is the free energy of a mixture of isotropic liquids. We choose it to be the Landau mean field free energy density

$$f_{\text{mix}}(\phi) = \frac{A}{2}(\phi-\phi_0)^2 + \frac{B}{4}(\phi-\phi_0)^4. \tag{3}$$

The coefficients A and B determine the properties of the bulk phases. For a nematic emulsion (i.e., two coexisting phases) A must be negative.

$f_{\text{ani}}(\phi,Q)$ in Eq. (2) is the free energy describing the nematic ordering of liquid crystals. We use the Landau-de Gennes expression [30]

$$f_{\text{ani}}(\phi,Q) = A_0\phi^2\left[\frac{1}{2}\left(1-\frac{\eta(\phi)}{3}\right)Q_{\mu\nu}^2 - \frac{\eta(\phi)}{3}Q_{\mu\nu}Q_{\nu\rho}Q_{\rho\mu} + \frac{\eta(\phi)}{4}(Q_{\mu\nu}^2)^2\right]. \tag{4}$$

(Greek subscripts will be used to represent Cartesian directions and the usual summation over repeated indices is assumed.) Equation (4) describes a first order, isotropic-nematic transition at $\eta(\phi)=2.7$ and A_0 is a constant. Following other studies [31,32] we weight $f_{\text{ani}}(\phi,\mathbf{Q})$ by $A_0\phi^2$, since only the liquid crystal molecules in the nematic phase will give this contribution to the free energy. For lyotropic liquid crystal mixtures we assume a linear relationship between η and ϕ [14,31–34] of the form

$$\eta = \eta_0 + \eta_s(\phi - \bar{\phi}) \tag{5}$$

to account for the dependence of the strength of the nematic ordering—which increases with increasing η—on the number of liquid crystal molecules. η_0, η_s, and $\bar{\phi}$ are constants which determine the boundary of the coexistence region. Examples of typical phase diagrams for a symmetric binary mixture are shown in Fig. 1. Figure 1(a) is the phase diagram for $A_0=1.5$, $\eta_0=2.6$, $\eta_s=0.3$, and $\bar{\phi}=0.5$. For $A<0$ there is two-phase coexistence between two isotropic phases. For $\eta_0=2.7$ [Fig. 1(b)], however, there is a first order transition at $A=0$ to two-phase coexistence between a nematic and an isotropic phase. The full line is the lattice Boltzmann simulation results, and the square symbols refer to a double-tangent calculation [34]. Results from the lattice Boltzmann simulations and the double-tangent construction are compared and shown to agree well. Slight differences between the two methods of calculation seen in Fig. 1(b) are due to the surface tension term included in the lattice Boltzmann calculations, and to the approximation of a uniaxial director field employed in the double-tangent construction.

In Eq. (1) f_{el} is the analogue in the $\mathbf{Q}$-tensor formalism of the Frank elastic free energy density. It gives the energy cost due to any elastic distortion in the director field,

$$f_{\text{el}} = \frac{K_1}{2}(\partial_\alpha Q_{\beta\gamma})^2 + \frac{K_2}{2}(\partial_\alpha Q_{\alpha\gamma})(\partial_\beta Q_{\beta\gamma}) + \frac{K_3}{2}Q_{\alpha\beta}(\partial_\alpha Q_{\gamma\epsilon}) \times (\partial_\beta Q_{\gamma\epsilon}), \tag{6}$$

where the K_i are elastic constants. In this work we use the one elastic constant approximation $K_1 \equiv K > 0$ and $K_2 = K_3 = 0$. This corresponds to having all three Frank elastic constants (splay, bend, and twist) equal [30].

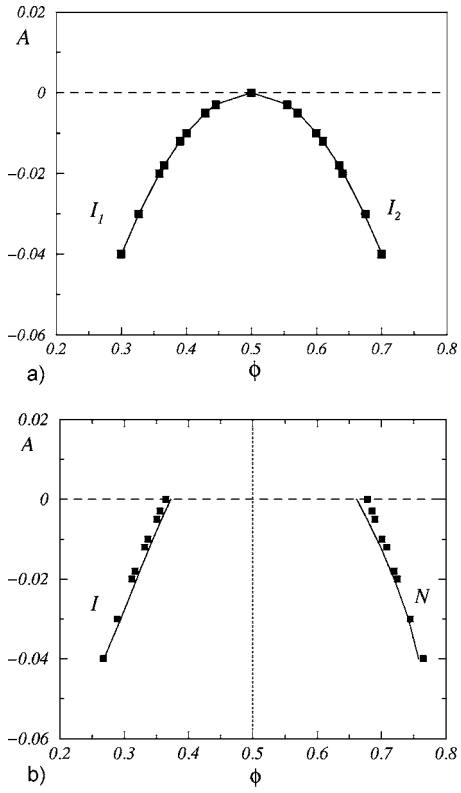

FIG. 1. Phase diagram of the binary isotropic–liquid crystal mixture described by the bulk free energy given in Eqs. (2)–(4). (a) $\eta_0=2.6$, $A_0=1.5$, $\phi_0=0.5$. Below the critical temperature two isotropic liquid phases I_1 and I_2 coexist. (b) $\eta_0=2.7$, $A_0=1.5$, $\phi_0=0.5$. There is a first order transition at $A=0$ to a region where an isotropic phase I and a nematic phase N coexist. The solid line is the lattice Boltzmann results and the symbols refer to the double-tangent calculation.

The contribution to the volume free energy which arises from an electric field $\vec{E}$ is of the form [30]

$$f_E = -\frac{\epsilon_a}{12\pi} E_\alpha Q_{\alpha\beta} E_\beta, \tag{7}$$

where ϵ_a is the dielectric anisotropy. We take $\epsilon_a>0$ corresponding to positive dielectric materials where the director field of the nematic liquid crystal component of the emulsion tends to align with the electric field.

Near an interface spatial variations occur in the two order parameters. The free energy contributions due to this are given by

$$f_{\kappa_\phi} = \frac{\kappa_\phi}{2}(\partial_\gamma \phi)^2 \tag{8}$$

and

$$f_W = L_0(\partial_\gamma \phi) Q_{\gamma\nu}(\partial_\nu \phi). \tag{9}$$

f_{κ_ϕ} penalizes gradients in concentrations. It ensures a smooth concentration profile across an interface, and provides a nonzero interfacial tension σ. f_W is a contribution that results from the coupling between the liquid crystal orientation and the concentration gradient at the interface between the two phases [14,27]. L_0, the cross-gradient coefficient, encourages the director to be aligned parallel ($L_0>0$) or perpendicular ($L_0<0$) to the gradient in ϕ at the interface.

If the liquid crystal is to be anchored at a bounding surface, we add a free energy

$$f_a = \tfrac{1}{2}\alpha_s (Q_{\alpha\beta} - Q^0_{\alpha\beta})^2, \tag{10}$$

where α_s controls the strength of the pinning and $Q^0_{\alpha\beta} = S_0(n^0_\alpha n^0_\beta - \delta_{\alpha\beta}/3)$, with n^0_α the preferred direction for the director at the boundary and S_0 determining the magnitude of surface order.

Minimizing the free energy with respect to concentration leads to the chemical potential

$$\mu = \frac{\delta \mathcal{F}}{\delta \phi} = [A(\phi-\phi_0) + B(\phi-\phi_0)^3] + \frac{\delta f_{\text{ani}}}{\delta \phi} - \kappa_\phi(\partial^2_\nu \phi) - 2L_0[(\partial_\gamma \partial_\nu \phi) Q_{\gamma\nu} + (\partial_\gamma \phi)(\partial_\nu Q_{\gamma\nu})]. \tag{11}$$

Phase equilibrium requires that μ is constant in equilibrium.

The thermodynamic contribution to the pressure tensor is

$$P_{\alpha\beta} = \Pi_{\alpha\beta} + \sigma_{\alpha\beta} + \tau_{\alpha\beta}, \tag{12}$$

where

$$\Pi_{\alpha\beta} = -\left(\frac{\delta \mathcal{F}}{\delta \phi}\phi - \mathcal{F}\right)\delta_{\alpha\beta} - \frac{\delta \mathcal{F}}{\delta(\partial_\beta \phi)}\partial_\alpha \phi - \frac{\delta \mathcal{F}}{\delta(\partial_\beta Q_{\gamma\nu})}\partial_\alpha Q_{\gamma\nu} \tag{13}$$

and $\sigma_{\alpha\beta}$ and $\tau_{\alpha\beta}$ are the contributions to the stress tensor which result from the liquid crystalline order. These parts of the stress tensor were derived phenomenologically in Ref. [29]. $\sigma_{\alpha\beta}$ is given by

$$\sigma_{\alpha\beta} = -P_0\delta_{\alpha\beta} - \xi H_{\alpha\gamma}\left(Q_{\gamma\beta} + \tfrac{1}{3}\delta_{\gamma\beta}\right) - \xi\left(Q_{\alpha\gamma} + \tfrac{1}{3}\delta_{\alpha\gamma}\right)H_{\gamma\beta} + 2\xi\left(Q_{\alpha\beta} + \tfrac{1}{3}\delta_{\alpha\beta}\right)Q_{\gamma\epsilon}H_{\gamma\epsilon}, \tag{14}$$

and the antisymmetric stress, $\tau_{\alpha\beta}$ is

$$\tau_{\alpha\beta} = Q_{\alpha\gamma}H_{\gamma\beta} - H_{\alpha\gamma}Q_{\gamma\beta}. \tag{15}$$

P_0 is the isotropic pressure and ξ is a constant that depends on the molecular details of a given liquid crystal [29]. $H_{\alpha\beta}$ is the molecular field which is defined in the following section.

B. The hydrodynamic equations of motion

We consider isothermal processes at constant volume. The equation of motion for the liquid crystal order parameter $\mathbf{Q}$ (symbols in boldface denote tensors quantities) can be written [29]

$$(\partial_t + u_\gamma \partial_\gamma)\mathbf{Q} - \mathbf{S}(\mathbf{W},\mathbf{Q}) = \Gamma \mathbf{H}, \tag{16}$$

where Γ is a collective rotational diffusion constant. The first two terms on the left-hand side of Eq. (16) correspond to the material derivative describing the time dependence of a quantity advected by a fluid with velocity $\vec{u}$. This is generalized for anisotropic molecules by a further term

$$\mathbf{S}(\mathbf{W},\mathbf{Q}) = (\xi\mathbf{D}+\mathbf{\Omega})(\mathbf{Q}+\mathbf{I}/3) + (\mathbf{Q}+\mathbf{I}/3)(\xi\mathbf{D}-\mathbf{\Omega}) - 2\xi(\mathbf{Q}+\mathbf{I}/3)\mathrm{Tr}(\mathbf{QW}), \quad (17)$$

where $\mathbf{D}=(\mathbf{W}+\mathbf{W}^T)/2$ and $\mathbf{\Omega}=(\mathbf{W}-\mathbf{W}^T)/2$ are the symmetric and antisymmetric parts, respectively, of the velocity gradient tensor, $W_{\alpha\beta}=\partial_\beta u_\alpha$ and $\mathbf{I}$ is the unit tensor. $\mathbf{S}(\mathbf{W},\mathbf{Q})$ takes into account the rotation of the rodlike molecules by flow gradients.

The orientational order parameter evolves in such a way as to lower the free energy, but it must do so subject to the constraint that it remains traceless. This is ensured by choosing the term on the right-hand side of Eq. (16), which is known as the molecular field, $\mathbf{H}$, to be

$$\mathbf{H} = -\left\{\frac{\delta\mathcal{F}}{\delta\mathbf{Q}} - \frac{1}{3}\mathbf{I}\mathrm{Tr}\frac{\delta\mathcal{F}}{\delta\mathbf{Q}}\right\}. \quad (18)$$

By performing the functional derivatives of the different contributions to the free energy we obtain

$$(H_{\mathrm{bulk}})_{\alpha\beta} \equiv (H_{\mathrm{ani}})_{\alpha\beta} = A_0\phi^2\left[-\left(1-\frac{\eta(\phi)}{3}\right)Q_{\alpha\beta} + \eta(\phi)\times\left(Q_{\alpha\mu}Q_{\mu\beta} - \frac{1}{3}\delta_{\alpha\beta}Q_{\nu\mu}Q_{\mu\nu}\right) - \eta(\phi)Q_{\alpha\beta}Q_{\nu\mu}Q_{\mu\nu}\right], \quad (19)$$

$$(H_{\mathrm{el}})_{\alpha\beta} = K\partial_\gamma\partial_\gamma Q_{\alpha\beta}, \quad (20)$$

$$(H_a)_{\alpha\beta} = -\alpha_s(Q_{\alpha\beta}-Q^0_{\alpha\beta}), \quad (21)$$

$$(H_W)_{\alpha\beta} = -L_0\left((\partial_\alpha\phi)(\partial_\beta\phi) - \frac{\delta_{\alpha\beta}}{3}(\partial_\mu\phi\partial_\mu\phi)\right), \quad (22)$$

$$(H_E)_{\alpha\beta} = \frac{\epsilon_a}{12\pi}\left(E_\alpha E_\beta - \frac{1}{3}\delta_{\alpha\beta}E^2\right). \quad (23)$$

The equation of motion for the concentration ϕ is a convection-diffusion equation of Cahn-Hilliard type,

$$\partial_t\phi + \partial_\alpha(\phi u_\alpha) = M\nabla^2\mu, \quad (24)$$

where M is a mobility constant which controls the diffusion. This equation states that the order parameter is advected by the fluid flow and responds to chemical potential gradients by diffusion.

The fluid velocity, in turn, obeys the continuity and Navier-Stokes equations

$$\partial_t\rho + \partial_\alpha\rho u_\alpha = 0, \quad (25)$$

$$\rho(\partial_t + u_\beta\partial_\beta)u_\alpha = \partial_\beta(\sigma_{\alpha\beta}) + \partial_\beta(\tau_{\alpha\beta}) + \partial_\beta(\Pi_{\alpha\beta}) + \eta_V\partial_\beta[\partial_\alpha u_\beta + \partial_\beta u_\alpha + (1-3\partial_\rho P_0)\partial_\gamma u_\gamma\delta_{\alpha\beta}], \quad (26)$$

where ρ is the fluid density and η_V is the fluid viscosity.

III. LATTICE-BOLTZMANN ALGORITHM FOR NEMATIC EMULSION HYDRODYNAMICS

The equations of motion for the binary mixture of a nematic and an isotropic phase Eq. (16) and Eqs. (24)–(26) are solved by using a lattice Boltzmann scheme. This is based on previous algorithms for a binary fluid [35,36] and for liquid crystal hydrodynamics [37,38]. The approach reproduces the equations of motion to second order in the lattice spacing.

In Sec. III A we present a description of how the lattice Boltzmann algorithm can be extended to model isotropic-nematic mixtures. We have found that spurious velocities, which arise as a result of discretization errors at places where there are gradients in the order parameters, lead to artifacts in the simulation results. Therefore, in Sec. III B we describe, following Wagner [39], a modified scheme that reduces the spurious velocities by a factor of $\sim 10^3$.

A. The lattice Boltzmann algorithm

The lattice Boltzmann algorithm is defined in terms of a set of partial distribution functions defined on each lattice site $\mathbf{x}$. For the isotropic-nematic binary mixture three sets of distribution functions are needed, namely, $f_i(\mathbf{x})$, $h_i(\mathbf{x})$, and $\mathbf{G}_i(\mathbf{x})$, where i labels lattice directions from the site $\mathbf{x}$. Physical variables are related to the distribution functions by

$$\rho = \sum_i f_i, \quad \phi = \sum_i h_i, \quad \mathbf{Q} = \sum_i \mathbf{G}_i. \quad (27)$$

The $\mathbf{G}_i$'s are, like $\mathbf{Q}$, symmetric and traceless tensors, with two independent components in two dimensions and five in three dimensions.

Each direction i is associated with a velocity vector $\mathbf{e}_i$. We choose a 15-velocity model on a cubic lattice with velocity vectors $\mathbf{e}_i=(\pm1,0,0)$, $(0,\pm1,0)$, $(0,0,\pm1)$, $(\pm1,\pm1,\pm1)$, and (0, 0, 0). Hence the fluid momentum is given by

$$\rho u_\alpha = \sum_i f_i \mathbf{e}_{i\alpha}. \quad (28)$$

The distribution functions f_i, h_i, and $\mathbf{G}_i$ evolve in a time step Δt according to the lattice Boltzmann equations,

$$f_i(\mathbf{x}+\mathbf{e}_i\Delta t, t+\Delta t) - f_i(\mathbf{x},t) = \frac{\Delta t}{2}[C_{fi}(\mathbf{x},t,f_i) + C_{fi}(\mathbf{x}+\mathbf{e}_i\Delta t, t+\Delta t, f_i^*)], \quad (29)$$

$$h_i(\mathbf{x}+\mathbf{e}_i\Delta t, t+\Delta t) - h_i(\mathbf{x},t) = \frac{\Delta t}{2}[C_{hi}(\mathbf{x},t,h_i) + C_{hi}(\mathbf{x}+\mathbf{e}_i\Delta t, t+\Delta t, h_i^*)], \quad (30)$$

$$\mathbf{G}_i(\mathbf{x}+\mathbf{e}_i\Delta t, t+\Delta t) - \mathbf{G}_i(\mathbf{x},t) = \frac{\Delta t}{2}[C_{\mathbf{G}i}(\mathbf{x},t,\mathbf{G}_i) + C_{\mathbf{G}_i}(\mathbf{x}+\mathbf{e}_i\Delta t, t+\Delta t, \mathbf{G}_i^*)]. \quad (31)$$

The left-hand sides of these expressions represent a streaming step with velocity $\mathbf{e}_i$ and the right-hand sides a collision step. f_i^*, h_i^*, and $\mathbf{G}_i^*$ are first order approximations to

$f_i(\mathbf{x}+\mathbf{e}_i t)$, $h_i(\mathbf{x}+\mathbf{e}_i t)$ and $\mathbf{G}_i(\mathbf{x}+\mathbf{e}_i t)$, respectively. They are derived by using just $\Delta t\ C_{fi}(\mathbf{x},t,f_i)$ on the right-hand side of Eq. (29) with similar substitutions for Eqs. (30) and (31). This discretization is similar to a predictor-corrector scheme. It removes lattice viscosity terms to second order and gives improved stability. The collision operators in Eqs. (29)–(31) are taken to have the form of a single relaxation time Boltzmann equation, together with forcing terms

$$C_{fi}(\mathbf{x},t,f_i) = -\frac{1}{\tau_f}[f_i(\mathbf{x},t) - f_i^{\mathrm{eq}}(\mathbf{x},t,\{f_i\})] + p_i(\mathbf{x},t,\{f_i\}) + F_i(\mathbf{x},t,\{f_i\}), \tag{32}$$

$$C_{hi}(\mathbf{x},t,h_i) = -\frac{1}{\tau_h}[h_i(\mathbf{x},t) - h_i^{\mathrm{eq}}(\mathbf{x},t,\{h_i\})], \tag{33}$$

$$C_{\mathbf{G}i}(\mathbf{x},t,\mathbf{G}_i) = -\frac{1}{\tau_G}[\mathbf{G}_i(\mathbf{x},t) - \mathbf{G}_i^{\mathrm{eq}}(\mathbf{x},t,\{\mathbf{G}_i\})] + \mathbf{M}_i(\mathbf{x},t,\{\mathbf{G}_i\}). \tag{34}$$

The conservation laws for the order parameters, and the required equations of motion, follow by imposing suitable constraints on the equilibrium distribution functions, f_i^{eq}, h_i^{eq}, and $\mathbf{G}_i^{\mathrm{eq}}$ and the driving terms, p_i, F_i, and $\mathbf{M}_i$. The equilibrium distributions functions are constrained by

$$\sum_i f_i^{\mathrm{eq}} = \rho, \quad \sum_i f_i^{\mathrm{eq}} e_{i\alpha} = \rho u_\alpha, \quad \sum_i f_i^{\mathrm{eq}} e_{i\alpha} e_{i\beta} = -\sigma_{\alpha\beta} + \rho u_\alpha u_\beta, \tag{35}$$

$$\sum_i h_i^{\mathrm{eq}} = \phi, \quad \sum_i h_i^{\mathrm{eq}} e_{i\alpha} = \phi u_\alpha,$$

$$\sum_i h_i^{\mathrm{eq}} e_{i\alpha} e_{i\beta} = M\mu\delta_{\alpha\beta} + \phi u_\alpha u_\beta,$$

$$\sum_i \mathbf{G}_i^{\mathrm{eq}} = \mathbf{Q}, \quad \sum_i \mathbf{G}_i^{\mathrm{eq}} e_{i\alpha} = \mathbf{Q}u_\alpha, \quad \sum_i \mathbf{G}_i^{\mathrm{eq}} e_{i\alpha} e_{i\beta} = \mathbf{Q}u_\alpha u_\beta. \tag{36}$$

The forcing terms are chosen to obey

$$\sum_i p_i = 0, \quad \sum_i p_i e_{i\alpha} = \partial_\beta \tau_{\alpha\beta}, \quad \sum_i p_i e_{i\alpha} e_{i\beta} = 0, \tag{37}$$

$$\sum_i F_i = 0, \quad \sum_i F_i e_{i\alpha} = \partial_\beta \Pi_{\alpha\beta}, \quad \sum_i F_i e_{i\alpha} e_{i\beta} = 0, \tag{38}$$

$$\sum_i \mathbf{M}_i = \Gamma \mathbf{H}(\mathbf{Q}) + \mathbf{S}(\mathbf{W},\mathbf{Q}) \equiv \hat{\mathbf{H}}, \quad \sum_i \mathbf{M}_i e_{i\alpha} = \left(\sum_i \mathbf{M}_i\right) u_\alpha. \tag{39}$$

The second moment of f_i^{eq} controls the liquid crystal stress tensor, $\sigma_{\alpha\beta}$, whereas the moments of p_i impose the antisymmetric part of the stress tensor, $\tau_{\alpha\beta}$. The first moment of F_i is equal to $\partial_\beta \Pi_{\alpha\beta}$ [see Eq. (13)]. This derivative can usefully be simplified by noting that

$$\begin{aligned} -\partial_\beta \Pi_{\alpha\beta} &= \partial_\alpha(\phi\mu - \mathcal{F}) + \partial_\beta \frac{\delta\mathcal{F}}{\delta\partial_\beta Q_{\gamma\nu}} \partial_\alpha Q_{\gamma\nu} + \frac{\delta\mathcal{F}}{\delta\partial_\beta Q_{\gamma\nu}} \partial_\alpha \partial_\beta Q_{\gamma\nu} \\ &\quad + \partial_\beta \frac{\delta\mathcal{F}}{\delta\partial_\beta \phi} \partial_\alpha \phi + \frac{\delta\mathcal{F}}{\delta\partial_\beta \phi} \partial_\alpha \partial_\beta \phi \\ &= -\left(\frac{\partial\mathcal{F}}{\partial Q_{\gamma\nu}} - \partial_\beta \frac{\delta\mathcal{F}}{\delta\partial_\beta Q_{\gamma\nu}}\right) \partial_\alpha Q_{\gamma\nu} \\ &\quad - \left(\frac{\partial\mathcal{F}}{\partial\phi} - \partial_\beta \frac{\delta\mathcal{F}}{\delta\partial_\beta \phi}\right) \partial_\alpha \phi + \partial_\alpha(\mu\phi), \\ &= H_{\gamma\nu} \partial_\alpha Q_{\gamma\nu} + (\partial_\alpha \mu)\phi. \end{aligned} \tag{40}$$

Conditions (35)–(39) can be satisfied, as is usual in lattice Boltzmann schemes, by writing the equilibrium distribution functions and forcing terms as polynomial expansions in the velocity [40]

$$f_i^{\mathrm{eq}} = A_s + B_s e_{i\alpha} u_\alpha + C_s u^2 + D_s u_\alpha u_\beta e_{i\alpha} e_{i\beta} + E_{s\alpha\beta} e_{i\alpha} e_{i\beta}, \tag{41}$$

$$h_i^{\mathrm{eq}} = H_s + I_s e_{i\alpha} u_\alpha + Y_s u^2 + Q_s u_\alpha u_\beta e_{i\alpha} e_{i\beta}, \tag{42}$$

$$\mathbf{G}_i^{\mathrm{eq}} = \mathbf{J}_s + \mathbf{K}_s e_{i\alpha} u_\alpha + \mathbf{L}_s u^2 + \mathbf{N}_s u_\alpha u_\beta e_{i\alpha} e_{i\beta}, \tag{43}$$

$$p_i = T_s \partial_\beta \tau_{\alpha\beta} e_{i\alpha}, \quad F_i = T_s \partial_\beta \Pi_{\alpha\beta} e_{i\alpha}, \quad \mathbf{M}_i = \mathbf{R}_s + \mathbf{S}_s u_\alpha e_{i\alpha}, \tag{44}$$

where $s = e_{i\alpha} e_{i\beta} \in \{0,1,2\}$ identifies separate coefficients for different absolute values of the velocities. Suitable choices for the coefficients are

$$A_2 = \sigma_{\gamma\gamma}/30, \quad A_1 = A_2, \quad A_0 = \rho - 14A_2,$$

$$B_2 = \rho/24, \quad B_1 = 8B_2,$$

$$C_2 = -\rho/24, \quad C_1 = 2C_2, \quad C_0 = -2\rho/3,$$

$$D_2 = \rho/16, \quad D_1 = 8D_2,$$

$$E_{2\alpha\beta} = \tfrac{1}{16}\left[\sigma_{\alpha\beta} - \left(\tfrac{1}{3}\sigma_{\gamma\gamma}\right)\delta_{\alpha\beta}\right], \quad E_{1\alpha\beta} = 8E_{2\alpha\beta},$$

$$H_1 = H_2, \quad H_0 = \phi - 14H_2, \quad H_2 = M\mu/10,$$

$$I_2 = \phi/24, \quad I_1 = 8I_2,$$

$$Y_2 = -\phi/24, \quad Y_1 = 2Y_2, \quad Y_0 = -2\phi/3,$$

$$Q_2 = \phi/16, \quad Q_1 = 8Q_2,$$

$$\mathbf{J}_0 = \mathbf{Q}, \quad \mathbf{K}_2 = \mathbf{Q}/24, \quad \mathbf{K}_1 = 8\mathbf{K}_2,$$

$$\mathbf{L}_2 = -\mathbf{Q}/24, \quad \mathbf{L}_1 = 2\mathbf{L}_2, \quad \mathbf{L}_0 = -2\mathbf{Q}/3,$$

$$\mathbf{N}_2 = \mathbf{Q}/16, \quad \mathbf{N}_1 = 8\mathbf{N}_2,$$

$$\mathbf{R}_2 = \hat{\mathbf{H}}/15, \quad \mathbf{R}_1 = \mathbf{R}_2 = \mathbf{R}_0,$$

$$\mathbf{S}_2 = \hat{\mathbf{H}}/24, \quad \mathbf{S}_1 = 8\mathbf{S}_2,$$

$$T_2 = 1/24, \quad T_1 = 8T_2. \tag{45}$$

B. Reduction of the spurious velocities

Note that the lattice Boltzmann scheme introduced in Sec. III A is slightly different from that described in Ref. [37]. Specifically, we introduce the $\partial_\beta \Pi_{\alpha\beta}$ term as a forcing term rather than adding $\Pi_{\alpha\beta}$ to $\sigma_{\alpha\beta}$ in the second moment constraint for the f_i^{eq} distributions [see Eqs. (13) and (14), respectively, and compare with Eq. (II.6) in Ref. [37]]. This is to overcome the problem of spurious velocities. At equilibrium, in a system with no forcing, the fluid velocity must be zero. However, using most standard lattice Boltzmann algorithms, the velocity profiles calculated in equilibrium show spurious velocities near interfaces. As the concentration gradient between the two phases increases the spurious velocities increase in magnitude. For a nematic emulsion such spurious velocities affect the director alignment at the drop interface, which, in turn, leads to unphysical results. In Ref. [39] it was shown that, for the case of a standard binary fluid, spurious velocities are related to numerical errors introduced by the first order upwind finite difference scheme and that they can be avoided by a careful choice of the discretization of the stress tensor and of the gradient of the concentration order parameter.

It is this observation that we exploit by including $\partial_\beta \Pi_{\alpha\beta}$ as a forcing term rather than in the second moment of the pressure tensor as detailed above. This enables us to ensure that the pressure tensor and the chemical potential are discretized in the same way. As the emulsion approaches equilibrium the molecular field and the derivative of the chemical potential, Eq. (40) vanish and $\partial_\beta \Pi_{\alpha\beta}$ becomes negligible. This reduces the spurious velocities by a factor of $\sim 10^3$ in equilibrium. (An estimate of the spurious velocities off equilibrium is hard as they are masked by the primary flow.) A simpler version of this scheme, for a fluid comprising only a liquid crystalline component, has recently been used to reduce spurious velocities in blue phase hydrodynamic flows [38].

C. Simulation parameters

We now list the simulation parameters we shall use and map them, where possible, to physical values. We consider $\eta_0=2.7$; $A_0=1.5$ and $\phi_0=0.5$ giving the phase diagram shown in Fig. 1(b). We choose $A=-0.016$, $B=0.8$, $\bar{\phi}=0.5$, and $\eta_s=0.3$. We also use $\tau_f=2.4$, $\tau_h=0.2$, $\tau_G=1.5$, $\Gamma=0.2$, $M=5.0$, and $\epsilon_a=10.35$. The most important parameters which control the shapes of the isotropic drops are the surface tension coefficient κ_ϕ, set equal to 0.025 in simulation units, the cross-gradient coefficient L_0, chosen to be between -0.02 for strong normal anchoring and -0.01 for weak anchoring, and the liquid crystal elastic constant K, which lies between 10^{-3} and 10^{-1}.

Although most of the results will be reported in terms of dimensionless variables it is of interest to discuss a possible mapping of the simulation parameters to physical values. We take the spacing between lattice sites to correspond to 0.1 μm and each time step in the simulation to correspond to 10^{-6} s. The simulation density $\rho=2$ is mapped onto 10^3 kg m^{-3}. An elastic constant $K=10^{-2}$ in simulation units then corresponds to 10^{-11} N which is a typical value for liquid crystals. We estimate the anchoring strength as

$$W = \frac{\int dV f_W}{\int_{S_d} dS} = \frac{\int dxdz L_0(\partial_\gamma \phi) Q_{\gamma\nu}(\partial_\nu \phi)}{\Gamma_d}, \tag{46}$$

where S_d denotes the surface of a drop and Γ_d its circumference. For strong anchoring we set $L_0=-0.02$, and for weak anchoring $L_0=-0.01$, both resulting in $W \sim 10^{-6}$ J m^{-2}, which is a physically realistic value [41,42]. The surface tension is calculated from

$$\sigma = \frac{\int dV f_{\kappa_\phi}}{\int_{S_d} dS} = \frac{\int dxdz \frac{\kappa_\phi}{2}(\partial_\gamma \phi)^2}{\Gamma_d}. \tag{47}$$

We are restricted for stability reasons to values of surface tension less than $\sim 10^{-4}$ in simulation units. This corresponds to a physical value $\sim 10^{-6}$ J m^{-2} which are too small compared to usual surface tensions $\sim (10^{-2}-10^{-3})$ J m^{-2} [41,42] but could be achieved by addition of a surfactant.

IV. SIMULATION RESULTS

In this section we present the results of simulating a drop of an isotropic fluid in a nematic liquid crystal medium, with an average liquid crystal concentration of $\sim 60\%$. We use the lattice Boltzmann algorithm summarized in Sec. III to solve the equations of motion for the nematic emulsion described in Sec. II. We first consider the equilibrium drop shapes and director configuration in the absence of an electric field. We then consider two problems where the drop moves; switching under an applied electric field and motion towards inhomogeneous boundaries. We shall consider the case where the director field prefers to be normal to the drop surface.

Equilibrium in zero applied electric field: First we consider the case in which there is no applied electric field. An isotropic drop of radius $R=60$ lattice units is initialized at the center of a simulation box of size $200 \times 1 \times 200$. Periodic boundary conditions are imposed in all directions; therefore the problem is two dimensional (the drops are cylindrical with circular cross section in the xz plane). Each simulation is run to equilibrium for about 300 000 time steps. (Note that we ran simulations with one-half the resolution finding the same phenomenology.)

The equilibrium shape of the drop is affected by several factors, in particular the surface tension, σ, the liquid crystal elastic constant, K and the anchoring strength of the director at the drop surface, W. Typical values of these parameters found in the literature [41,42] are $\sigma=10^{-2}$ J m^{-2},

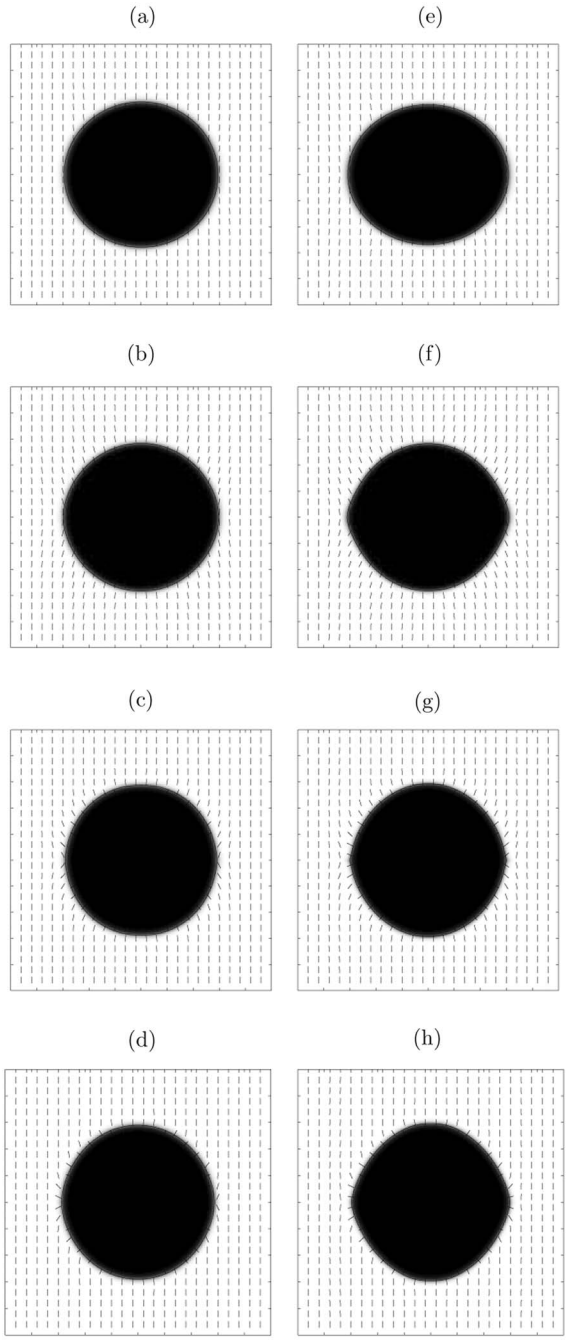

FIG. 2. (Color online) Equilibrium shapes and director configuration for isotropic drop of radius 60 in a nematic host. First column, $|L_0/\kappa_\phi|=0.4$. Second column, $|L_0/\kappa_\phi|=0.8$. (a) $K=10^{-1}$, $WR/K=0.009$, (b) $K=10^{-2}$, $WR/K=0.154$, (c) $K=10^{-3}$, $WR/K=2.27$, (d) $K=10^{-4}$, $WR/K=27.1$, (e) $K=10^{-1}$, $WR/K=0.026$, (f) $K=10^{-2}$, $WR/K=0.50$, (g) $K=10^{-3}$, $WR/K=6.42$, (h) $K=10^{-4}$, $WR/K=68.7$.

$K=10^{-11}$ N and $W=10^{-7}$ to 10^{-3} J m^{-2} depending on the nature, quality and treatment of the surface. We introduce the dimensionless ratio WR/K which measures the strength of the surface anchoring energy relative to the bulk director deformations [30]. In general, the drop size observed in nematic emulsions is between 1–10 μm. Therefore, possible values of WR/K corresponding to experiment are within the range $(10^{-2}-10^{3})$. When $WR/K<1$ the anchoring is considered weak. Under these conditions one does not observe clear defects at the equator of the droplet, nor large deformations in the surrounding nematic phase. When $WR/K\gg 1$, however, the anchoring is strong and can deform the director field. We estimate W, which is the free energy per unit area of isotropic-nematic interface, using Eq. (46). For strong anchoring and small surface tension, the droplet shape is deformed [27] and another important dimensionless number is W/σ. To understand the effect of changing W/σ it is more convenient, and equivalent, to use the ratio of simulation parameters $|L_0/\kappa_\phi|$.

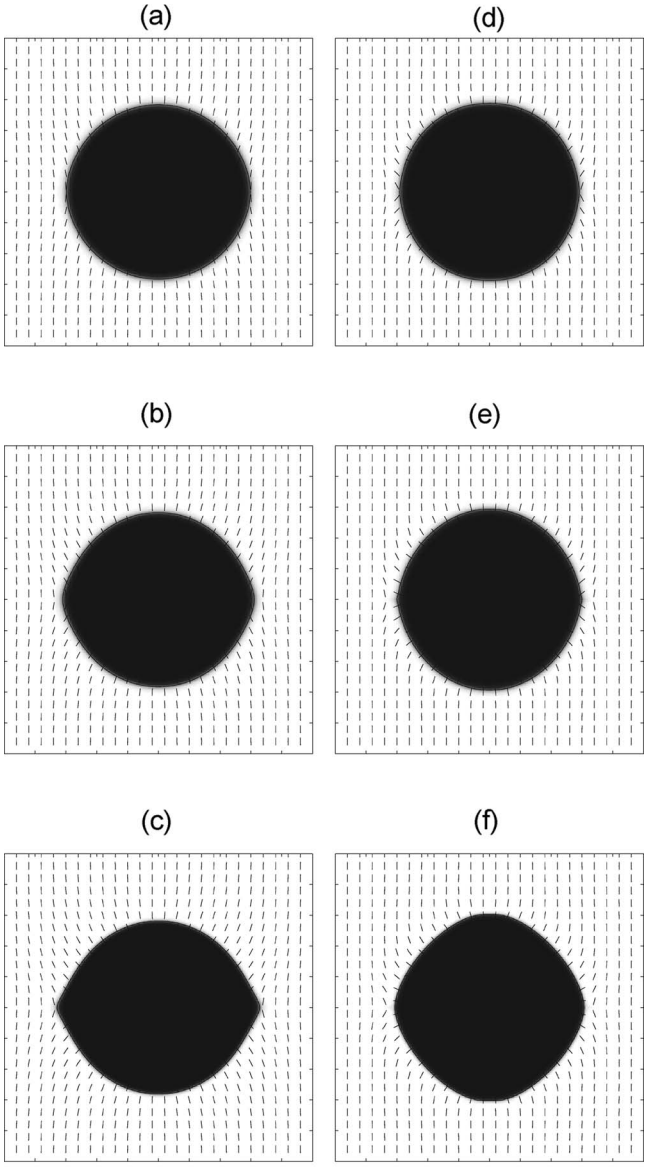

FIG. 3. Drop of radius 60 at three values of the dimensionless number $|L_0/\kappa_\phi|$. First column corresponds to $K=10^{-2}$ and the second column corresponds to $K=10^{-3}$. $|L_0/\kappa_\phi|$ increases down a column as $|L_0/\kappa_\phi|=0.4$, 0.8, and 1.33.

The effect of modifying WR/K is illustrated in Fig. 2 for two different values of $|L_0/\kappa_\phi|$. In Figs. 2(a)–2(d) $|L_0/\kappa_\phi|$

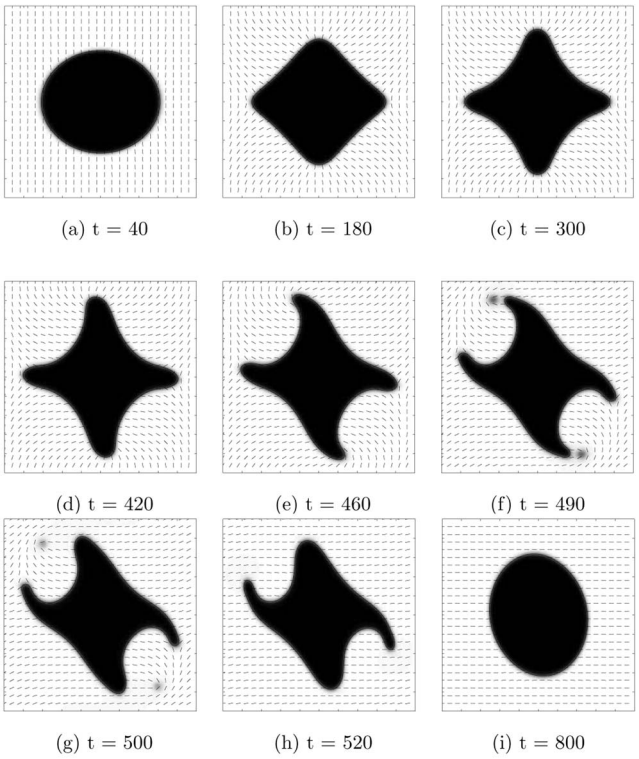

FIG. 4. Snapshots in time of an isotropic drop in a nematic host after a horizontal electric field is switched on. Boundary conditions are periodic in both directions and time shown is in thousands of simulation steps. $K=10^{-1}$, $|L_0/\kappa_\phi|=0.8$, $WR/K=0.026$.

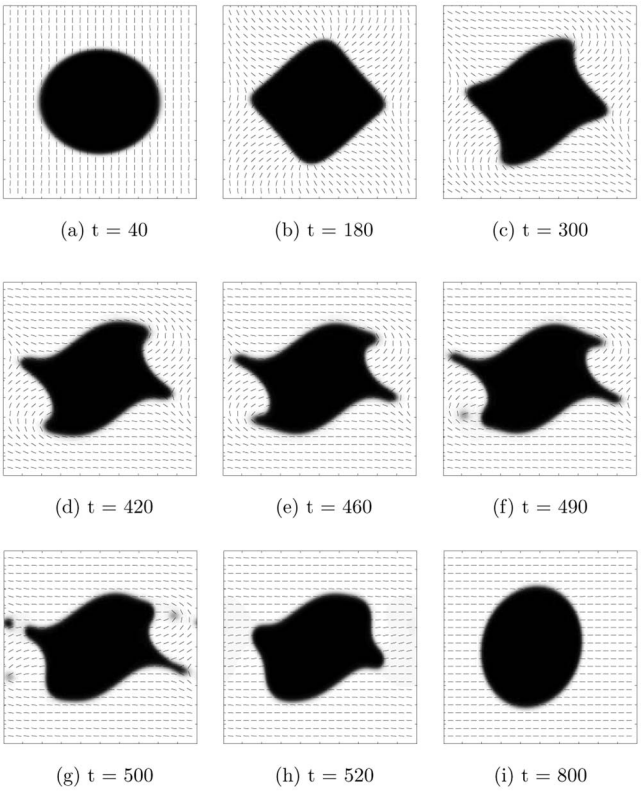

FIG. 5. Snapshots in time of an isotropic drop in a nematic host after a horizontal electric field is switched on. Boundary conditions are periodic in both directions and time shown is in thousands of simulation steps. $K=10^{-1}$, $|L_0/\kappa_\phi|=0.8$, $WR/K=0.026$. The director field is initiated with a random angle between $-1°$ and $1°$ to the x axis.

$=0.4$. For Fig. 2(a) $WR/K=0.009$, which means that the elastic energy dominates the surface energy. Thus the director does not deform around the drop and no distortion is observed in the nematic phase at its surface. The nematic director field is tangent to the drop at the equator and no defects can be observed. For slightly larger WR/K, Fig. 2(b), small perturbations are introduced into the director field at the surface of the drop but still no clear defects can be seen. However, in Figs. 2(c) and 2(d) for $WR/K=2.27$ and 27.1, respectively, the surface energy dominates and the director field is well anchored at the surface of the drop. These configurations result in two defects of strength $-1/2$ positioned at opposite poles of the drop (corresponding to a Saturn ring defect in three dimensions). As seen in the figure, the ring defect does not lead to long-range director distortions, in agreement with its quadrupolar nature [2,43]. The director order parameter tends to zero at the defect core corresponding to the fluid being in the isotropic phase.

Figures 2(e)–2(h) show how the equilibrium drop shape and the director field vary with WR/K for a larger value of $|L_0/\kappa_\phi|=0.8$. The values of WR/K are given in the caption of the figure. The main effect of the larger value of $|L_0/\kappa_\phi|$ is that it is easier for the drop to distort to accommodate normal anchoring at the surface. For the smallest WR/K case, Fig. 2(e), the elastic constant is sufficiently large that it dominates the anchoring at the drop surface. For slightly smaller elastic constant, the anchoring strength is large enough compared to the surface tension to distort the circular shape of the drop, but it is still too weak to produce clear defects at the equator. For much larger WR/K, Fig. 2(h), the director can be easily deformed to satisfy the surface normal boundary condition and, therefore, the drop shape does not need to deform greatly.

Figure 3 shows a drop of radius 60 at equilibrium for two values of the elastic constant K. The dimensionless number $|L_0/\kappa_\phi|$ increases going down a column. As $|L_0/\kappa_\phi|$ increases the anchoring energy dominates over the surface tension and the drop distorts to more easily allow normal anchoring at its surface.

V. DYNAMICS IN AN APPLIED ELECTRIC FIELD

In this section we investigate the switching dynamics of an isotropic drop in a nematic host in the presence of an applied electric field. The direction of the applied field is chosen perpendicular to the initial orientation of the nematic bulk phase. We consider periodic boundary conditions in all directions. This means that the threshold voltage for the Freedericksz transition is zero. We consider the two equilibrated droplets shown in Figs. 2(e) and 2(f), respectively. Each has a radius $R=60$ lattice units in a system of size 200×200. Figure 4 shows the time evolution of a system with a large elastic constant ($WR/K=0.026$) when an electric field of magnitude $E=0.02$ (in simulation units) is applied

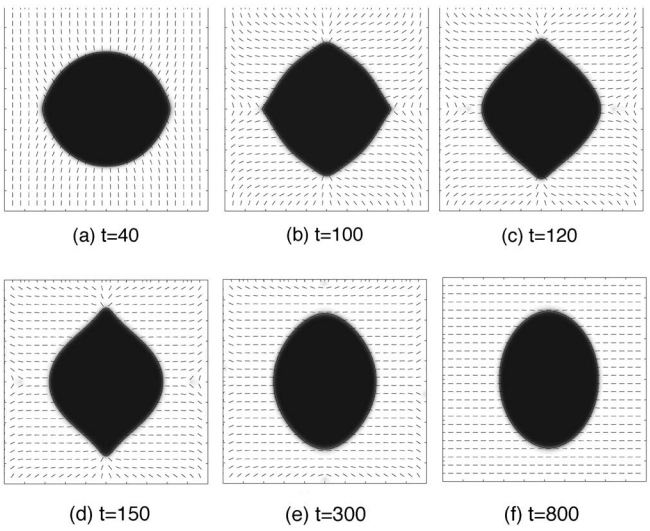

FIG. 6. Snapshots in time of an isotropic drop in a nematic host after a horizontal electric field is switched on. Periodic boundary condition in both directions and time is shown in thousands of simulation steps. $K=10^{-2}$, $|L_0/\kappa_\phi|=0.8$, $WR/K=0.50$.

across the cell. The behavior of the drop is surprisingly complex. The liquid crystal surrounding the drop starts to align along the direction of the applied field. This distorts the drop shape so as to satisfy the normal anchoring condition at the surface, with arms appearing along and perpendicular to the field direction. As the director field continues to rotate, defects are formed near the tips of the arms perpendicular to $\vec{E}$. They detach from the drop surface, move to the ends of the arms parallel to $\vec{E}$ and annihilate, Figs. 4(g)–4(i), allowing the drop to relax to its equilibrium shape, but perpendicular to its original position. The large distortions of the drop are allowed because the surface tension is small; this behavior is likely only to be seen in a physical system if surfactants are added.

We also note that the kinetic pathway shown in Fig. 4 depends substantially on the initial conditions used. If the director field is initialized by adding a random noise, uniformly distributed between $-1°$ and $1°$ to the x axis, the pathway is similar, as shown in Fig. 5, but the switching is approximately twice as fast. Note that the tilted droplet in the last frame of Fig. 5 does, in the end, relax to the same final condition as Fig. 4 but this is a long process as it corresponds to a tiny decrease in free energy.

If the director field is instead initialized with a pretilt of 5° with respect to the x axis the switching time is faster by an order of magnitude and the transient deformations reported in Figs. 4 and 5 disappear. This is because all the molecules rotate in the direction of the pretilt.

Figure 6 shows a system with a smaller elastic constant ($WR/K=0.50$) under the same electric field $E=0.02$. Now the switching pathway is different and depends crucially on the existence of neighboring drops (recall that we have periodic boundary conditions). In the majority of the cell the director quickly aligns with the field. However, because of the influence of the drop boundaries it does this by rotating in different directions leaving areas of distortion at the drop

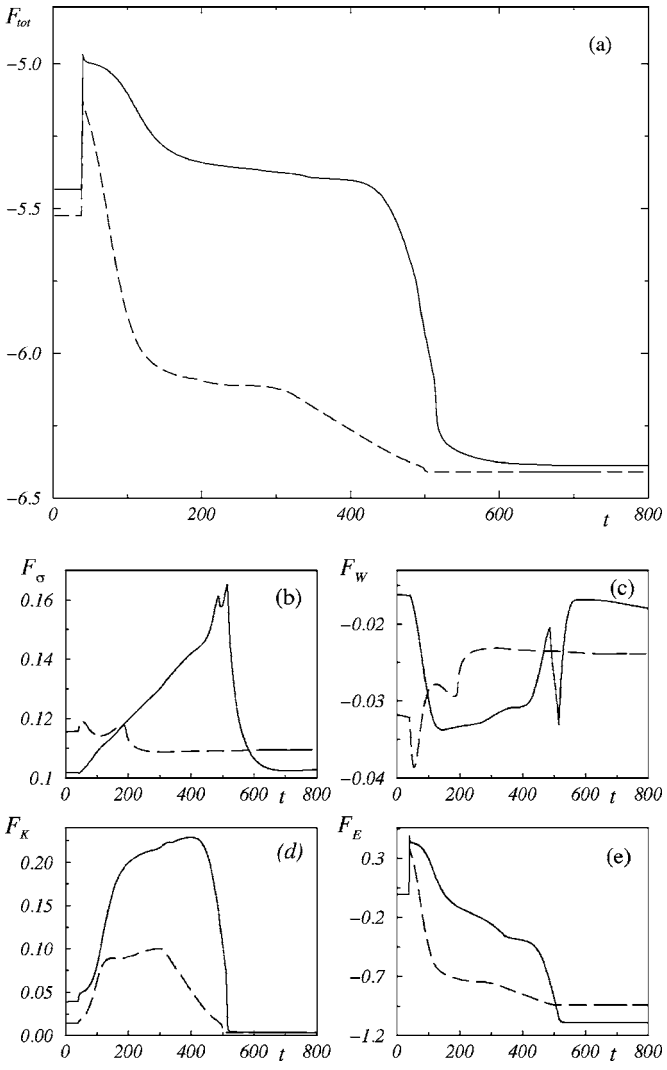

FIG. 7. Variation of the free energy with time for the switching process shown in Figs. 4 and 6: Solid line, $K=10^{-1}$ (Fig. 4); dashed line, $K=10^{-2}$ (Fig. 6). (a) Total free energy, $F_{\rm tot}$; (b) surface tension free energy, F_σ; (c) anchoring free energy, F_W; (d) elastic free energy, F_K; (e) electric field free energy, F_E. Time is shown in thousands of simulation steps and the free energy is in simulation units.

poles and equator and on the edges of the simulation box, i.e., the lines midway between the drops. These untwist by a unzipping mechanism caused by defects moving from the drop surface to midway between the drops.

Figure 7 compares the free energy contribution during the switching for the two systems in Figs. 4 and 6. The most important barrier that the system needs to overcome results from the elastic free energy. This is, as expected, larger for the drop in Fig. 4 which has a larger elastic constant. It takes longer for this barrier to be overcome and for the elastic energy to start to decrease to its final value. The large distortions of this drop are reflected in the peak in the surface tension free energy. For comparison, we simulated a nematic liquid crystal with periodic boundary conditions and same value of elastic constants and electric field. This aligns with the field in $\sim 4\times 10^5$ lattice Boltzmann iterations, so the emulsions both switch slightly faster. (Note that to observe

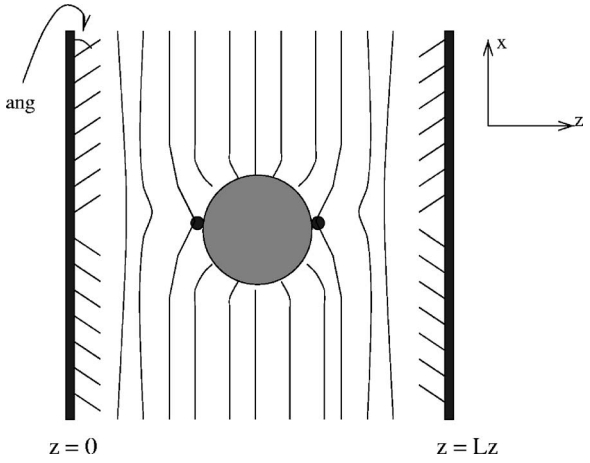

FIG. 8. A drop of an isotropic fluid is placed in a cell containing nematic liquid crystal. The director field is pinned at the boundary at an angle θ_p as shown in the diagram. ($\theta_p=20°$ is exaggerated in the schematic representation for clarity.)

switching with periodic boundary conditions for the pure nematic, the director must be initialized with a small, e.g., 10^{-6}, component along the field.)

VI. DYNAMICS IN A CELL WITH SURFACE PATTERNING

In this section we explore the dynamics of the drop when it is confined between two flat substrates at $z=0$ and $z=100$ that have different director alignment on their surfaces. We consider an isotropic drop of radius $R=30$ lattice units. Periodic boundary conditions are imposed along x and y. In the simulation we set the boundary condition at the two surfaces [$\mathbf{Q}^0$ in Eq. (10)] to give an angle $\theta_p=+20°$ to the x axis for $x>50$ and $\theta_p=-20°$ for $x\leqslant 50$. A schematic diagram illustrating this initial configuration is shown in Fig. 8. Normal anchoring is imposed at the surface of the drop.

The normal anchoring condition at the drop surface produces two $-1/2$ defects located at the poles of the drop. As is seen from Fig. 8, this leads to a mismatch between the director configuration at the $z=0$ boundary and that imposed by the anchoring condition on the drop's surface. If the drop is fixed in its place, then the director would need to distort in order to satisfy both boundary conditions. This, however, costs substantial energy, especially for larger elastic constants. In order to minimize the elastic free energy the drop will move away from this side of the cell. Figure 9 shows this dynamic for elastic constant $K=0.05$. For $K=0.1$ the motion is similar but $\sim 10\%$ faster.

It is interesting to turn off the back flow to assess its contribution to the dynamics. This can be done by decoupling the evolution of the fluid from the liquid crystal order parameter. We find that the drop has moved slower by 6%.

VII. CONCLUSIONS

In this paper we have developed a lattice Boltzmann algorithm to model the equilibrium and dynamical properties

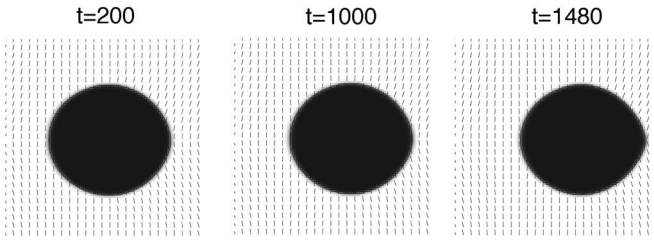

FIG. 9. Time evolution of an isotropic drop in a nematic host confined between two flat substrates with different director alignment on their surfaces. $K=0.05$, $|L_0/\kappa_\phi|=0.8$. Time is shown in thousands of simulation steps.

of a nematic emulsion where one or more microdroplets of an isotropic fluid are immersed in a nematic liquid crystal. Equilibrium is described by a Landau-de Gennes free energy functional and the hydrodynamics by the Beris-Edwards equations of motion written in terms of the Q tensor. This is a demanding numerical task because of the complexity of the equations involved. Large enough drops must be simulated to avoid lattice pinning effects and, to obtain correct interface dynamics, it proved important to use the ideas of Wagner [39] to minimize spurious velocities.

We first applied the algorithm to study the director field of the nematic fluid around a two-dimensional isotropic droplet of radius R for different values of the liquid crystal elastic constant K, surface tension σ and anchoring strength of the director at the isotropic-nematic interface W. As WR/K is increased two defects of strength $-1/2$ appear at the equator of the drop. As W/σ increases the drop shape becomes increasingly distorted.

We then investigated two problems where hydrodynamics might play a role. We followed the transient dynamics of an array of drops as the director was switched through 90° by an applied electric field. For a large elastic constant there was a pronounced deformation of the droplet shape during the switching. For a smaller elastic constant the switching was, as expected, faster and the drop shape less perturbed.

We also showed that the algorithm is able to follow the way in which a drop of isotropic fluid moves towards a patterned surface to minimize the elastic free energy. Here back flow does not affect the dynamics significantly.

The results are a first step towards understanding more fully the rheology of liquid crystal emulsions and their possible uses in devices. Investigating the behavior of liquid crystal drops in an isotropic host and extensions from nematic to cholesteric ordering are also feasible. There are several directions for development. For example, it would be desirable to be able to treat larger values of surface tension. Moreover, although the current code is fully three dimensional, obtaining results in three dimensions is very demanding of computational resources.

ACKNOWLEDGMENTS

The authors would like to thank C. Care and A. Dupuis for helpful discussions. One of the authors (N.S.) acknowledges the support of Sultan Qaboos University, Oman.

[1] P. Poulin, H. Stark, T. C. Lubensky, and D. A Weitz, Science **275**, 1770 (1997).
[2] P. Poulin and D. A. Weitz, Phys. Rev. E **57**, 626 (1998).
[3] J.-C. Loudet, P. Barols, and P. Poulin, Nature (London) **407**, 611 (2000).
[4] M. Yada, J. Yamamoto, and H. Yokoyama, Phys. Rev. Lett. **92**, 185501 (2004).
[5] I. I. Smalyukh, O. D. Lavrentovich, A. N. Kuzmin, A. V. Kachynski, and P. N. Prasad, Phys. Rev. Lett. **95**, 157801 (2005).
[6] V. G. Nazarenko, A. B. Nych, and B. I. Lev, Phys. Rev. Lett. **87**, 075504 (2001).
[7] T. Bellini, M. Caggioni, N. A. Clark, F. Mantegazza, A. Maritan, and A. Pelizzola, Phys. Rev. Lett. **91**, 085704 (2003).
[8] I. I. Smalyukh, S. Chernyshuk, B. I. Lev, A. B. Nych, U. Ognysta, V. G. Nazarenko, and O. D. Lavrentovich, Phys. Rev. Lett. **93**, 117801 (2004).
[9] G. De. Filpo, J. Lanzo, F. P. Nicoletta, and G. Chidichimo, J. Appl. Phys. **84**, 3581 (1998).
[10] O. Mondain-Monval, J. C. Dedieu, T. Gulik-Krzywicki, and P. Poulin, Eur. Phys. J. B **12**, 167 (1999).
[11] Y. Gu and N. L. Abbott, Phys. Rev. Lett. **85**, 4719 (2000).
[12] J. C. Loudet and P. Poulin, Phys. Rev. Lett. **87**, 165503 (2001).
[13] J. Fukuda and H. Yokoyama, Eur. Phys. J. E **4**, 389 (2001).
[14] T. Araki and H. Tanaka, Phys. Rev. Lett. **93**, 015702 (2004).
[15] C. S. Park, N. A. Clark, and R. D. Noble, Phys. Rev. Lett. **72**, 1838 (1994).
[16] D. Andrienko, G. Germano, and M. P. Allen, Phys. Rev. E **63**, 041701 (2001).
[17] M. Allen, Comput. Phys. Commun. **169**, 433 (2005).
[18] J. L. Billeter and R. A. Pelcovits, Phys. Rev. E **62**, 711 (2000).
[19] J. I. Fukuda, M. Yoneya, and H. Yokoyama, Phys. Rev. E **65**, 041709 (2002).
[20] H. Stark, Eur. Phys. J. B **10**, 311 (1999).
[21] S. Grollau, N. L. Abbott, and J. J. de Pablo, Phys. Rev. E **67**, 011702 (2003).
[22] N. M. Silvestre, P. Patricio, M. Tasinkevych, D. Andrienko, and M. M. Telo da Gamma, J. Phys.: Condens. Matter **16**, 51921 (2004).
[23] O. Guzman, E. B. Kim, S. Grollau, N. L. Abbott, and J. J. de Pablo, Phys. Rev. Lett. **91**, 235507 (2003).
[24] S. Grollau, E. B. Kim, O. Guzman, N. Abbott, and J. J. de Pablo, J. Chem. Phys. **119**, 2444 (2003).
[25] R. W. Ruhwandl and E. M. Terentjev, Phys. Rev. E **56**, 5561 (1997).
[26] J. Fukuda, H. Stark, M. Yoneya, and H. Yokoyama, J. Phys.: Condens. Matter **16**, S1957 (2004).
[27] C. Care, I. Halliday, K. Good, and S. V. Lishchuk, Phys. Rev. E **67**, 061703 (2003).
[28] S. V. Lishchuk and C. M. Care, Phys. Rev. E **70**, 011702 (2004).
[29] A. N. Beris and B. J. Edwards, *Thermodynamics of Flowing Systems* (Oxford University Press, Oxford, 1994).
[30] P. G. de Gennes and J. Prost, *The Physics of Liquid Crystals*, 2nd ed. (Clarendon, Oxford, 1993).
[31] A. Matsuyama and T. Kato, J. Chem. Phys. **105**, 1654 (1996).
[32] A. Matsuyama, R. M. L. Evans, and M. E. Cates, Eur. Phys. J. E **9**, 79 (2002).
[33] P. D. Olmsted and C. Y. David Lu, Phys. Rev. E **60**, 4397 (1999).
[34] A. Matsuyama, R. M. L. Evans, and M. E. Cates, Eur. Phys. J. E **9**, 89 (2002).
[35] M. R. Swift, E. Orlandini, W. R. Osborn, and J. M. Yeomans, Phys. Rev. E **54**, 5041 (1996).
[36] E. Orlandini, M. R. Swift, and J. M. Yeomans, Europhys. Lett. **32**, 463 (1995).
[37] C. Denniston, D. Marenduzzo, E. Orlandini, and J. M. Yeomans, Philos. Trans. R. Soc. London, Ser. A **362**, 1762 (2004).
[38] A. Dupuis, D. Marenduzzo, E. Orlandini, and J. M. Yeomans, Phys. Rev. Lett. **95**, 097801 (2005).
[39] A. J. Wagner, Int. J. Mod. Phys. B **17**, 193 (2003).
[40] S. Chen and G. D. Doolen, Annu. Rev. Fluid Mech. **30**, 329 (1998).
[41] J. Cognard, Molecular crystals and liquid crystals, Supp. 1, London, 1982.
[42] V. J. Anderson, E. M. Terentjev, S. P. Meeker, J. Crain, and W. C. K. Poon, Eur. Phys. J. E **4**, 11 (2001).
[43] T. C. Lubensky, D. Pettey, N. Currier, and H. Stark, Phys. Rev. E **57**, 610 (1998).